Conformer-specific vibronic spectroscopy and vibronic coupling in a flexible bichromophore: Bis-(4-hydroxyphenyl)methane

Chirantha P. Rodrigo,[1,a)] Christian W. Müller,[1,b)] Nathan R. Pillsbury,[1,c)] William H. James III,[1,d)] David F. Plusquellic,[2,e)] and Timothy S. Zwier[1,e)]
[1]*Department of Chemistry, Purdue University, West Lafayette, Indiana 47907-2084, USA*
[2]*Biophysics Group, Physical Measurement Laboratory, National Institute of Standards and Technology, Gaithersburg, Maryland 20899-8443, USA*

(Received 12 February 2011; accepted 1 April 2011; published online 28 April 2011)

The vibronic spectroscopy of jet-cooled bis-(4-hydroxyphenyl)methane has been explored using fluorescence excitation, dispersed fluorescence (DFL), UV–UV hole-burning, UV depletion, and fluorescence-dip infrared spectroscopies. Calculations predict the presence of three nearly isoenergetic conformers that differ in the orientations of the two OH groups in the *para* positions on the two aromatic rings (labeled uu, dd, and ud). In practice, two conformers (labeled A and B) are observed, with S_0–S_1 origins at 35 184 and 35 209 cm^{-1}, respectively. The two conformers have nearly identical vibronic spectra and hydride stretch infrared spectra. The low-frequency vibronic structure is assigned to bands involving the phenyl torsions (T and $\bar{T}$), ring-flapping (R and $\bar{R}$), and butterfly (β) modes. Symmetry arguments lead to a tentative assignment of the two conformers as the C_2 symmetric uu and dd conformers. The S_0–S_2 origins are assigned to bands located 132 cm^{-1} above the S_0–S_1 origins of both conformers. DFL spectra from the S_2 origin of the two conformers display extensive evidence for vibronic coupling between the two close-lying electronic states. Near-resonant coupling from the S_2 origin occurs dominantly to S_1 $\bar{R}^1$ and S_1 $\bar{R}^1\beta^1$ levels, which are located –15 and +31 cm^{-1} from it. Unusual vibronic activity in the ring-breathing (ν_1) and ring-deformation (ν_{6a}) modes is also attributed to vibronic coupling involving these Franck–Condon active modes. A multimode vibronic coupling model is developed based on earlier theoretical descriptions of molecular dimers [Fulton and Gouterman, J. Chem. Phys. **35**, 1059 (1961)] and applied here to flexible bichromophores. The model is able to account for the ring-mode activity under conditions in which the S_2 origin is strongly mixed (60%/40%) with S_1 $\overline{6a}^1$ and $\bar{1}^1$ levels. The direct extension of this model to the $T/\bar{T}$ and $R/\bar{R}$ inter-ring mode pairs is only partially successful and required some modification to lower the efficiency of the S_1/S_2 mixing compared to the ring modes. © *2011 American Institute of Physics*. [doi:10.1063/1.3580901]

I. INTRODUCTION

Bis-(4-hydroxyphenyl)methane [b4HPM, Fig. 1(a)] is a flexible bichromophore containing two *para*-cresol (*p*-cresol) [Fig. 1(b)] units sharing the same methyl group. It is a close analog of diphenylmethane [DPM, Fig. 1(c)],[1,2] differing from it by addition of two OH groups in the *para* positions on both rings. In the ground electronic state, the OH groups add two further flexible coordinates (OH internal rotation) to the two phenyl torsional coordinates already present in DPM. In DPM, the symmetry of the phenyl rings produces two enantiomeric minima that are spectroscopically indistinguishable from one another. Our recent study of bis-(2-hydroxyphenyl)methane [b2HPM, Fig. 1(d)], placed the two OH groups *ortho* to the methylene where they can interact with one another, producing both OH···O and OH···π bound conformers.[3] In b4HPM, a structural isomer of b2HPM, the two OH groups are placed in the *para* positions on the rings, too far away to interact directly with one another. As shown in Fig. 2, the asymmetry of the OH groups produces four minima differing in the relative orientations of the OH groups either pointing up (u) toward or down (d) away from the bridging methylene group. Three of these (uu, dd, and ud/du) are spectroscopically distinguishable, thereby facilitating a detailed characterization of the torsional potential energy surface by selective excitation and spectroscopic characterization of the observed conformational isomers.

One of our motivations in carrying out this study is that b4HPM, such as DPM,[1,2] is a model system for state-selective studies of excitonic effects, with two *p*-cresol ultraviolet chromophores in close proximity to one another. We therefore anticipate the presence of two close-lying excited states, whose energy separation and degree of localization or delocalization depends sensitively on the relative orientation of two chromophores and the magnitude of the

a)Present address: Department of Chemistry, University of Southern California, Los Angeles, California 90089-1062, USA.
b)Present address: Ruhr University Bochum, Department of Physics and Chemistry 2, D-44780 Bochum, Germany.
c)Present address: BP Naperville, 150 W Warrenville Rd, Naperville, Illinois 60563, USA.
d)Present address: SCHOTT North America, Inc., 400 York Avenue, Duryea, Pennsylvania 18642, USA.
e)Authors to whom correspondence should be addressed. Electronic mail: Zwier@purdue.edu and david.plusquellic@nist.gov.

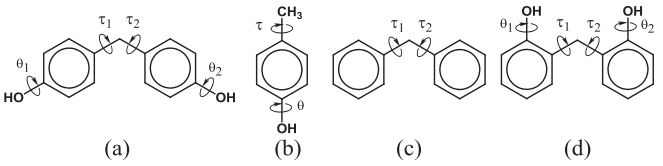

FIG. 1. Structure and torsional coordinates of (a) b4HPM, (b) the single-chromophore analog of b4HPM, *p*-cresol, (c) DPM, and (d) b2HPM.

electronic coupling between them. In this circumstance, vibronic effects are anticipated to be significant, since the two electronic states have vibrational manifolds that are intermingled with one another at energies not far above the S_1 origin, where state-specific mixing can be probed.

In recent work on DPM,[1,2] we explored its vibronic and rotationally resolved spectroscopy in some detail under jet-cooled conditions. In that case, the splitting between the S_0–S_1 and S_0–S_2 origin transitions was 123 cm^{-1}. DPM retained C_2 symmetry in all three electronic states, with electronic excitation in S_1 and S_2 delocalized over the two rings. Dispersed fluorescence from the S_2 zero-point level showed clear signatures of vibronic coupling (sometimes referred to as "internal mixing")[4] between the S_2 zero-point level and nearby S_1 vibronic levels, reflecting the quantum character of the S_1 vibronic levels involved in the mixing through the $\Delta v = 0$ Franck–Condon (FC) emission back to corresponding levels in the ground state.

The state-selective view of vibronic coupling between the two states afforded by those studies provided a motivation for further exploration of other flexible bichromophores that differ from DPM in well-defined ways. Previous work on b2HPM was less revealing about vibronic effects than that in DPM, in part, because either large asymmetry (in the OH···O conformer) or weak intensity (OH···π conformer) made it difficult to identify and characterize the S_2 states. The present study of b4HPM does not suffer from such effects, and thus is a first example of substituted versions of diphenylmethane that possess conformational isomers, and thus provide conformation-specific access to different regions of the excited state torsional surfaces from each of the observed conformational minima. Relative to DPM, the magnitude of the electronic splitting and the vibrational frequencies of coupled modes are anticipated to change in ways that we hope will give an additional insight into the coupling between the vibronic states of the two electronic potential energy surfaces.

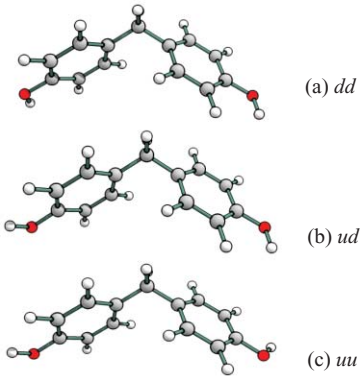

FIG. 2. Energy minimized structures of three conformations calculated with DFT/B3LYP/6–31+G(d) level of theory. Down–down (dd), up–up (uu), and up–down (ud) labels were assigned based on the direction of the OH group orientation as shown. Treated as rigid structures, the dd and uu conformations have C_2 symmetry, while ud has C_1 symmetry.

The present paper focuses attention on the vibronic spectroscopy of b4HPM. We use an array of single- and double-resonance techniques to characterize the ground and excited state surfaces, including fluorescence excitation (FE), dispersed fluorescence (DFL), UV–UV hole-burning (UVHB), and fluorescence-dip infrared (FDIR) (Ref. 5) spectroscopies. Elsewhere, we will report on high resolution UV spectra of several of the vibronic bands of both conformers,[6] and on stimulated emission pumping-population transfer spectra that determined the energy barriers and relative energies of the conformational minima of b4HPM.[7]

One of the significant advances in this work is the development of a multidimensional vibronic coupling model[8] applied earlier to excitonic effects in molecular dimers[9] and its application to flexible bichromophores. As we shall see, this model is able to account for unusual vibronic intensities involving the Franck–Condon active ring modes observed in the S_1 and S_2 origin emission spectra. The extension of this model to include the inter-ring torsion and ring-flapping modes is only partially successful, pointing the way for future work.

II. EXPERIMENTAL COMPUTATIONAL METHODS

A. Experiment

The experimental methods used to record FE, DFL, and UVHB spectra of b4HPM have been explained in detail elsewhere.[10] Only a brief explanation is presented here. A solid sample of b4HPM was purchased from SigmaAldrich[11] (98% purity) and used without further purification. The sample was heated to 140 °C and expanded into vacuum through a 500 μm diameter pulsed nozzle ($P_0 = 3$ bar He).

The frequency doubled output of a Nd:YAG-pumped dye laser (ScanMate and ScanMate Pro) is used as the fluorescence excitation light source (≈0.1 mJ/pulse). Fluorescence was detected with a photomultiplier tube (ETI 9318QB) using either a boxcar gated integrator (SR 250) or directly in a digital oscilloscope (Tektronix TDS 3052B) controlled by a data acquisition computer.

UV–UV hole-burning spectroscopy was used to record conformation-specific UV spectra. In this case, an ultraviolet hole-burning laser (0.2 mJ/pulse, 10 Hz) was fired 200 ns before the probe laser (0.1 mJ/pulse, 20 Hz), suitably overlapped in space to sample the same molecular population. The wavelength of the hole-burn laser was fixed on a transition of interest at an intensity sufficient to partially saturate the transition, thereby removing a measurable fraction of the ground state population. The UV probe laser was then tuned through the spectral region of interest, while the difference in the signal with and without the hole-burn laser was recorded, using active baseline subtraction in a gated integrator. All transitions sharing the same ground state level showed a nonzero

difference signal, thereby producing a conformation-specific UV spectrum.

If the hole-burn laser is tuned and the probe laser is fixed in wavelength, an alternative form of the hole-burning spectrum results that we call UV-depletion (UVD) spectroscopy. In the context of this work, the UVD spectra enabled us to look sensitively for small transitions that were hard to observe in the UVHB spectra.

DFL spectra were recorded using a Jobin Yvon 750i monochromator (0.75 m) and a charge coupled device camera (Andor series DU440BU2) operating at –75 °C temperature. The spectral resolution of the DFL spectra was about 6–8 cm^{-1} with 50–100 μm entrance slit widths.

Details of the FDIR spectra are included in the supplementary material.[5]

B. Computational methods

Starting structures for the low-lying minima of b4HPM were selected by performing AMBER (Ref. 12) force field calculations within the MACROMODEL (Ref. 13) suites of programs. Resulting geometries were then used as inputs for geometry optimizations with more accurate levels of theory. Both standard density functionals (B3LYP) (Ref. 14) and dispersion corrected functionals (M052-X,[15] ωB97X-D[16]) were used to compute energies of selected conformations. Two split valance basis sets (6–31+G* and 6–311G**) were employed using the GAUSSIAN 03 and GAUSSIAN 09 suites of programs.[17] Harmonic vibrational frequencies were also calculated at the same level of theory to confirm the absence of negative frequencies and to provide predictions for comparison with experiment. Excited state geometry optimizations were carried out with configuration interaction singles (CIS/6–311G**) method within the Q-CHEM computational package.[18] Vertical excitation energies were also computed with same levels of theories on optimized ground state geometries.

III. COMPUTATIONAL RESULTS

Optimized structures for the three low-energy conformers of b4HPM computed at the DFT B3LYP/6–31G* level of theory have already been shown in Fig. 2. There is little change in either the structure or vibrational frequencies between B3LYP and the two dispersion-corrected functionals used (Sec. II B). The uu and dd conformational minima have C_2 symmetry, while ud/du is C_1. The calculated inter-ring angle is 91 °, close to that found in DPM (93 °).

As in DPM, many of the high-frequency vibrations involving the ring modes of b4HPM come in symmetric/antisymmetric pairs that are sums and differences of modes identifiable in the "monomer" equivalent *p*-cresol. In most cases, the calculations predict ground state vibrational frequencies for each pair separated from one another by no more than a few cm^{-1}. In the C_2 symmetry conformers, they form an a/b symmetry pair, only one of which would appear as a dipole-allowed fundamental in the vibronic spectrum.

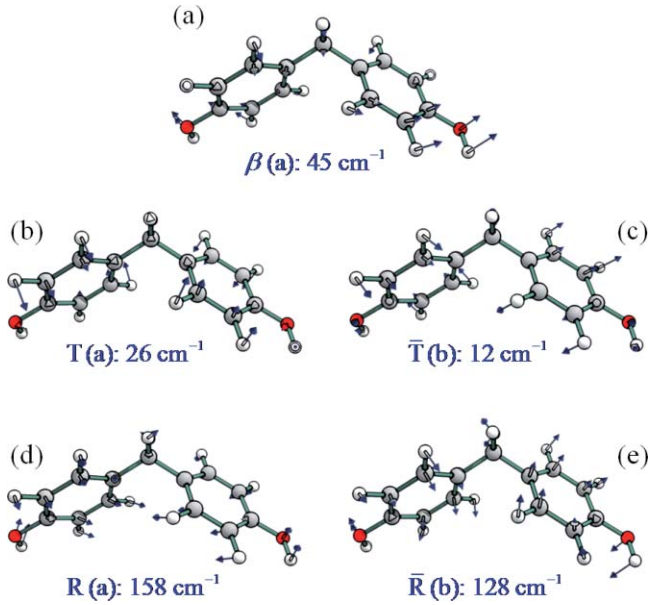

FIG. 3. Calculated form of the low-frequency vibrational modes of b4HPM(dd). (a) Butterfly (β), (b) symmetric phenyl torsion (T), (c) antisymmetric phenyl torsion ($\bar{T}$), (d) symmetric phenyl flap (R), (e) antisymmetric phenyl flap ($\bar{R}$). The symmetries of the modes in the C_2 point group and ground state vibrational frequencies are indicated.

The low-frequency modes in the conformers of b4HPM involve inter-ring motions that have close analogs in DPM.[1,2] Figure 3 plots the form of the five lowest-frequency modes of b4HPM, which play a prominent role in the spectroscopy. Once again, in the C_2 symmetry conformers, the $T/\bar{T}$ and $R/\bar{R}$ modes form a/b symmetry pairs that change the orientation of the phenyl rings with respect to one another. Again, if C_2 symmetry is maintained in the b4HPM conformers upon electronic excitation, only the T and R modes will have allowed fundamentals, while only the even overtones and combination bands of $\bar{T}$ and $\bar{R}$ should be allowed. The totally symmetric butterfly mode (β) lacks an antisymmetric partner, which instead corresponds to rotation about an axis perpendicular to the C_2 axis. In our study of DPM,[1,2] the $\bar{R}$ mode was labeled $\bar{\beta}$, which we now think is inappropriate given the form of the mode. The predicted frequencies of these modes are given in the figure for convenient comparison with experiment.

The form of the normal modes changes only slightly in the ud conformer, despite the fact that it strictly no longer has C_2 symmetry. As a result, it is questionable whether symmetry arguments can be used to definitely rule out this conformer's presence.

IV. EXPERIMENTAL RESULTS AND ANALYSIS

A. Fluorescence excitation, UVHB, and UVD spectra

The fluorescence excitation spectrum of b4HPM is shown in Fig. 4(a). The transition furthest to the red, at 35 184 cm^{-1}, is likely to be an $S_1 \leftarrow S_0$ origin transition of one of the conformers of b4HPM. It appears –147 cm^{-1} from the $S_1 \leftarrow S_0$ origin transition reported for *p*-cresol (35 331 cm^{-1}), which possesses the same (uncoupled) UV chromophore.[19,20]

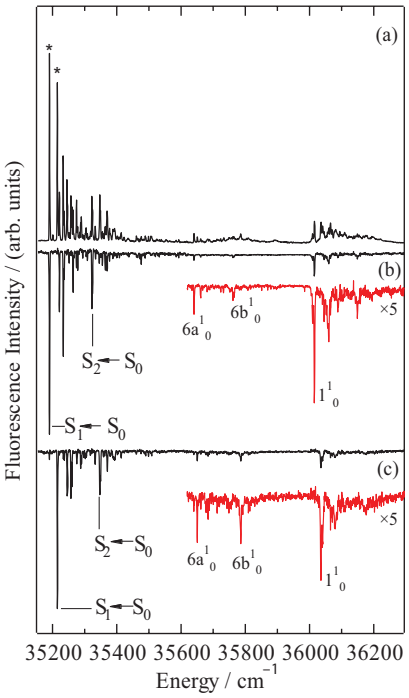

FIG. 4. (a) Fluorescence excitation spectrum of b4HPM in the (35 155–36 290) cm^{-1} spectral region. (b) and (c) UV–UV hole-burning spectra of conformers A and B, respectively. The two lowest electronic origin transitions $\tilde{A}\ ^1B(S_1) \leftarrow \tilde{X}\ ^1A(S_0)$ and $\tilde{B}\ ^1A(S_2) \leftarrow \tilde{X}\ ^1A(S_0)$ are labeled in the UV-HB spectrum of conformer A. Transitions used in UV-HB are labeled with asterisks in (a).

The overview UVHB spectra in Figs. 4(b) and 4(c) were recorded with the hole-burning laser fixed on the transitions marked by asterisks in Fig. 4(a). Under coldest conditions in the expansion, these two UVHB spectra account for essentially all observed transitions over the entire wavenumber region shown, establishing the presence of two conformers of b4HPM. The S_0–S_1 origin transitions of the two conformers (A at 35 184 cm^{-1} and B at 35 209 cm^{-1}) are separated from one another by 24.8 cm^{-1}. (We note that the vacuum corrected frequencies of A and B are 35 175 and 35 199 cm^{-1}, respectively).[6] Since, based on the calculations, we were anticipating the presence of a third conformer, careful searches were made for this conformer over a range of conditions, including the ones in which the expansion was warmer and hot bands could appear. Based on the vibronic analysis that follows, it was possible to account for all transitions as arising from these two conformers and their hot bands. Since high resolution spectra of most of the main bands in these spectra have been recorded,[6] it is unlikely that the bands are masked by an overlap with transitions from conformers A and B. We surmise on this basis that the transitions due to a third conformer, if it has bound levels at all, are too weak to be observed. This is a likely consequence of the small energy barriers separating the minima, enabling cooling to occur between them. Further studies of the two-dimensional (2D) torsional surface and measurement of the energy barriers separating the minima are left for future work.[7]

The insets in Figs. 4(b) and 4(c) show the higher-frequency region at a magnification five times than that in the origin region. Transitions due to prominent in-plane ring distortion (6*a*) and ring breathing (1) fundamentals are labeled in the spectrum, using the Varsanyi numbering scheme.[21]

Figures 5(a) and 5(b) show expanded views of the first 200 cm^{-1} of the UVHB spectra of conformers A and B of b4HPM. Both spectra exhibit extensive vibronic structure, most of which can be accounted for by analogy to DPM as fundamentals, overtones, and combination bands involving β, T, $\bar{T}$, and R, as indicated in the figure and summarized in Table I. DFL spectra (Sec. IV B) will confirm these assignments. Notably, the +43 cm^{-1} transition in both spectra is assigned as $\bar{T}^2_0$, with no measurable intensity at half this frequency where the fundamental would occur. However, UV-depletion spectroscopy can be used to look sensitively at high laser powers for even weak transitions in the conformation-specific UV spectrum. The UVD spectra in Figs. 5(c) and 5(d) show the clear presence of a very weak transition assignable to the $\bar{T}^1_0$ fundamental, appearing 21.5 cm^{-1} above the S_1 origin. This confirms the assignment of the +43 cm^{-1} transition to the $\bar{T}^2_0$ overtone. Furthermore, the $\bar{T}^1_1$ sequence band appears under warmer expansion conditions at +10.5 cm^{-1}, exactly where predicted based on its S_0 (11 cm^{-1}, Sec. IV B) and S_1 (21.5 cm^{-1}) frequencies. The high laser powers needed to observe the $\bar{T}^1_0$ fundamental, and the strong intensity of its first overtone, suggests that the $\bar{T}^1_0$ fundamental appears only by weak vibronic coupling with the S_2 state, consistent with the presence and retention of C_2 symmetry in S_0 and S_1 states.

UVHB and UVD scans of both observed conformers of b4HPM show two transitions shifted +132 and +134 cm^{-1} from the S_1 origin, which cannot be accounted for as combinations and overtones of T, $\bar{T}$, and β. Given the fact that DPM has its S_0–S_2 origin, $\tilde{B}^1A(S_2) \leftarrow \tilde{X}^1A(S_0)$, 123 cm^{-1} above the S_1 origin, it seemed plausible that these bands may be associated with S_0–S_2 origin transitions. As we shall shortly see, based on the DFL spectra, one of these bands is indeed the S_0–S_2 origin, while the other is the S_0–S_1 R^1_0 fundamental.

Fluorescence-dip infrared spectra have been recorded in the CH and OH stretch regions of the infrared. The spectra of the two conformers, shown in the supplementary material,[5] are nearly identical with one another, as might be expected given the subtle structural differences between the potential conformers (uu, ud, dd).

B. DFL spectra

1. S_1 origin DFL

DFL spectra of the $S_1 \leftarrow S_0$ origin bands of the two conformers of b4HPM are shown in Fig. 6. In the low-frequency region (shown in the inset), fundamentals due to the symmetric torsion (T, 21 cm^{-1}), butterfly (β, 45 cm^{-1}), and flapping (R, 155 cm^{-1}) modes are assignable based on analogy with DPM and close correspondence with calculated frequencies (Table II). The $\bar{T}^0_2$ overtone is also present at 25 cm^{-1}. The large drop in frequency in the butterfly and flapping mode frequencies from those in DPM ($\beta = 63$ cm^{-1}, $R = 223$ cm^{-1}) is a consequence of the larger reduced mass of these vibrations in the presence of the two oxygen atoms in *para* positions on

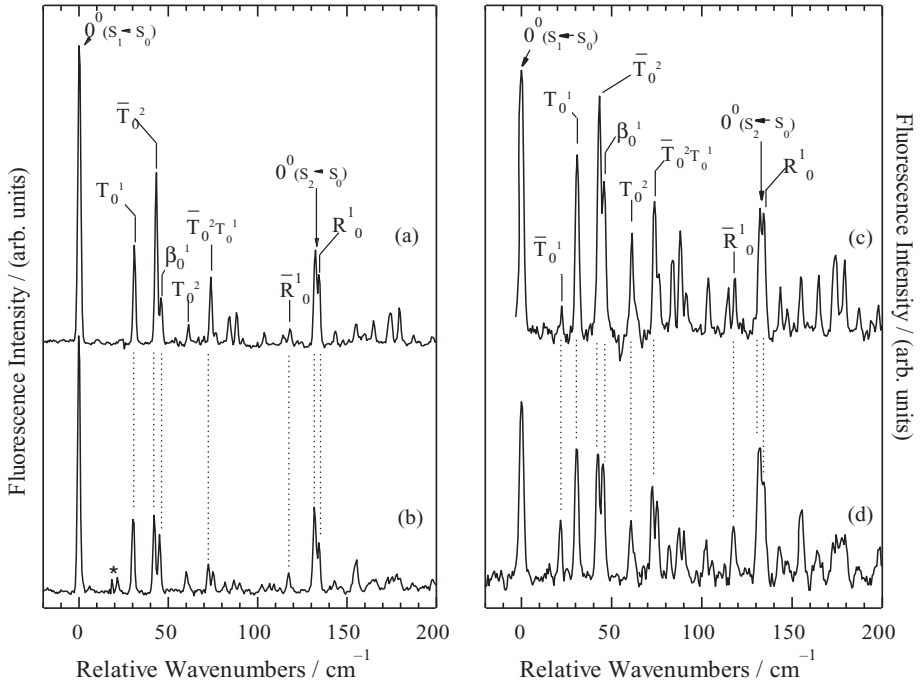

FIG. 5. UV-HB spectra of the low-frequency regions of (a) conformer A and (b) conformer B of b4HPM, plotted on a relative wavenumber scale for direct comparison with one another. Transitions labeled in the spectrum are assigned based on the comparison with DPM and DFL spectra, as detailed in the text. Corresponding transitions of conformer B are indicated with dotted lines. Asterisks in (b) show incomplete subtraction of signal in the UV–UV double resonance experiment. (c,d) Corresponding UV depletion spectra, showing weak transitions observable only under highly saturated conditions.

TABLE I. Frequencies and assignments of observed transitions in the FE spectra.

Expt. freq. Conf A (cm^{-1})	Expt. freq. Conf B (cm^{-1})	Assignment	Expt. freq. DPM[a] (cm^{-1})	CIS/6–311G(d,p) (symm) Unscaled frequencies (cm^{-1})			Symmetry	Expt. freq. p-cresol[b]
				dd (C_2)	ud (C_1)	uu (C_2)		
0	0	$(S_1 \leftarrow S_0)0^0$	0	…	…	…	A	…
…[c]	…[c]	$\bar{T}^1_0$	…	28.4	29.5	16.4	B	…
31	30	T^1_0	29	29.8	31.3	30.3	A	…
43.5	42	$\bar{T}^2_0$	43	…	…	…	A	…
46	45	β^1_0	~56[d]	48.5	48.6	47.3	…	…
61	60	T^2_0	54	…	…	…	A	…
74	75	$T^1_0 \bar{T}^2_0$	…	…	…	…	A	…
77	75	$T^1_0 \beta^1_0$	…	…	…	…	A	…
84	86	$\bar{T}^4_0$	…	…	…	…	A	…
88	90	β^2_0	…	…	…	…	A	…
104	102	$\bar{T}^2_1 T^2_0$	…	…	…	…	A	…
118	117	$\bar{R}^1_0$	…	126.8	126.6	120.2	B	…
132	132	$(S_2 \leftarrow S_0)0^0$	123	…	…	…	A	…
134	136	R^1_0	…	161.5	162.0	162.4	A	…
155.5	155.5	…	…	…	…	…	A	…
450	435	$6a^1_0$	…	…	…	…	A	$6a^1_0$
825	820	1^1_0	…	…	…	…	A	1^1_0

[a]Reference 1.
[b]Reference 18.
[c]$\bar{T}$ fundamental transition observed in UVD at 21.5 cm^{-1}.
[d]This value is approximate since the transition was not completely resolved.

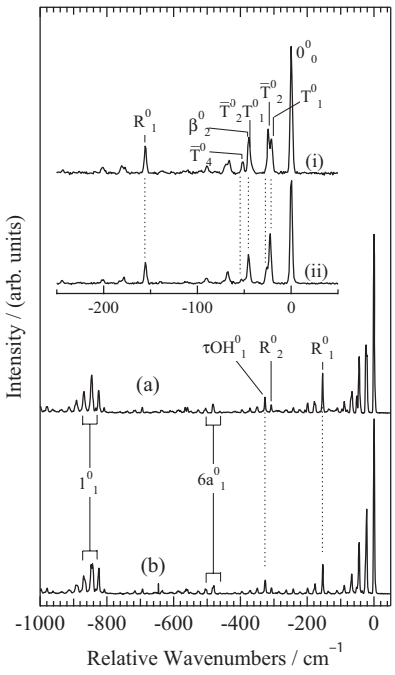

FIG. 6. $S_1 \leftarrow S_0$ origin dispersed fluorescence spectra of conformers (a) A and (b) B of b4HPM using 50 μm entrance slit on the monochromator. The inset shows an expanded view of the low-frequency region of the spectra taken with 10 μm entrance slit.

the ring. The small changes in T and $\bar{T}$ reflect the fact that the oxygen atoms are on the axes about which phenyl torsion occurs. We tentatively assign the weak band at 326 cm^{-1} to the fundamental of the symmetric out-of-plane torsion of the two OH groups (τOH) with calculated frequency of 333 cm^{-1}. The corresponding mode in phenol has been reported at 310 cm^{-1} by Kleinermanns *et al.*[22] The set of transitions near 850 cm^{-1} is in a region where one might anticipate the ring breathing mode (ν_1). However, only the *antisymmetric* ring breathing mode (in which one ring is expanding while the other is contracting) is identifiable in this frequency region amongst the calculated normal modes (861 cm^{-1}, b symmetry). Other in-plane ring deformation modes (e.g., 6*a*) are very weak in the S_1 origin emission spectrum, a point to which we will return later.

2. Symmetric torsion progression (T)

Figures 7(c) and 7(d) present the DFL spectra of the transitions 31 and 62 cm^{-1} above the S_1 origin of b4HPM(A), assigned as the T^1_0 and T^2_0 fundamentals. Franck–Condon fitting of the torsional progressions in these spectra, the 0^0 DFL spectrum [Fig. 7(b)] and the UVHB spectrum [Fig. 7(a)], reproduce the torsional intensities with a displacement parameter, D = 0.85.[23] These are values similar to those found for DPM.[1]

3. +43 and +46 cm^{-1} bands ($\bar{T}^2_0/\beta^1_0$)

DFL spectra of the +43 cm^{-1} transitions of A and B are shown in Figs. 8(a) and 8(b). The corresponding spectra of the +46 cm^{-1} bands are shown below them in Figs. 8(c) and 8(d). The qualitative appearance of the emission from these bands is consistent with their assignment as the $\bar{T}^2_0$ and β^1_0 transitions, respectively. The spectra from conformer B are easiest to interpret in this way. The B+43 cm^{-1} spectrum [Fig. 8(b)] has its strongest transition at –25 cm^{-1}, ascribable to the $\bar{T}^2_2$ transition. The tie lines in the figure highlight the progression in even quanta $\bar{T}^2_n$ that dominate the spectrum. In Fig. 8(d), strong transitions appear at (–44, –89, and –132) cm^{-1}, associated with a progression due to β^1_n, n = 1–3.

The fact that the antisymmetric torsion $\bar{T}$ appears only as an even overtone in both excitation and dispersed fluorescence is most consistent with the two observed conformers being the symmetric conformers uu and dd. The transition dipole moments determined by high resolution ultraviolet spectroscopy of the S_0–S_1 origins of the two conformers also points to this assignment,[6] which is discussed in more detail in Ref. 6.

Beyond the assignments themselves, however, aspects of the spectra in Fig. 8 are puzzling. Some of these intensity anomalies can be accounted for by invoking a 2:1 Fermi resonance between the β^1 and $\bar{T}^2$ upper levels, reflected in the presence of a strong $\bar{T}^2_2$ band appearing in emission from (nominally) β^1 [Fig. 8(d)]. Indeed, a quantitative analysis of this Fermi resonance mixing in conformer B (see supplementary material for details) yields best fit mixing parameters indicating a 75%/25% mixing of the two upper states.[5]

In addition, in both conformers, the $\Delta v = \pm 2$ transitions in $\bar{T}$ are much more intense than one would expect from normal Franck–Condon predictions in a nontotally symmetric vibration. This is especially the case in conformer A, where the $\Delta v = \pm 2$ transitions in Fig. 8(a) are significantly greater than their $\Delta v = 0$ counterpart. These same transitions in Fig. 8(c) show larger intensity than the β^1_1 transition.

Furthermore, emission from other bands in S_1 with $\bar{T}$ excitation shows similar trends. Under warm expansion conditions, a hot band grows in +10.5 cm^{-1} from the S_1 0^0_0 of A, assigned as the $\bar{T}^1_1$ sequence band. Its DFL spectrum is shown in Fig. 9. We observe a nearly pure progression in odd members of $\bar{T}^1_n$, with a $\bar{T}^1_3$ transition about two-thirds the intensity of its $\Delta v = 0$ counterpart $\bar{T}^1_1$. This is the case despite the fact that there is a firm evidence for the retention of C_2 symmetry, since the Δv = odd transitions are, at most, very weak relative to $\Delta v = 2$. Any Franck–Condon analysis with zero displacement along $\bar{T}$ fails miserably in accounting for the observed intensities in this progression. After careful consideration of possible interferences or artifacts, we conclude that these anomalous intensities involving the $\bar{T}$ progression are real signatures of vibronic coupling in b4HPM. We return to a further discussion of this point in Sec. V.

4. +132/134 cm^{-1} doublet ($S_2 0^0_0 / S_1 R^1_0$) and +117 cm^{-1} ($S_1 \bar{R}^1_0$)

The UVHB spectra in Fig. 5 show bands in both conformers 132 cm^{-1} above their respective S_0–S_1 origins, at about one-third the intensity, with shoulders just to the blue (134 cm^{-1} in A). The high resolution spectrum of the +132 cm^{-1}, to be reported in detail elsewhere,[6] is observed to have a transition dipole moment parallel to the C_2 axis (and

TABLE II. Prominent transitions in the dispersed fluorescence spectrum of the S_1 zero-point levels of conformers A and B of b4HPM, compared to DPM.

Expt. freq. (cm^{-1})				B3LYP/6–31+G* Freq (Symm) (cm^{-1})			
Conf A	Conf B	DPM[b]	Assignment[a]	dd	ud	uu	Symmetry
0	0	0	…	…	…	…	…
…	…	…	$\bar{T}_1^0$	11.5(B)	14.7(A)	14.4 (B)	…
20.7	22.3	19	T_1^0	26.0 (A)	24.8(A)	25.5(A)	…
24.4	26.1	31	$\bar{T}_2^0$	23(A)	29.4(A)	28.8(A)	A
…	36	…	$\bar{T}_2^0\bar{T}_1^0$	…	…	…	…
43	44	38	T_2^0	…	…	…	…
45	45.2	63	β_1^0	44.3(A)	44.9(A)	44.4(A)	A
51.7	52.9	…	$\bar{T}_4^0$	…	…	…	…
66	67.3	83	$T_1^0\beta_1^0$	…	…	…	…
69	72	…	$\bar{T}_2^0\beta_1^0$	…	…	…	…
90	90	126	β_2^0	…	…	…	…
108	110.7	…	$T_1^0\beta_2^0$	…	…	…	…
112	113.3	…	$\bar{T}_1^0\beta_2^0$	…	…	…	…
156	155.5	223	R_1^0	157.8(A)	157.5(A)	157.9(A)	A
177	178	…	$T_1^0R_1^0$	…	…	…	…
181	183.4	…	$\bar{T}_2^0R_1^0$	…	…	…	…
199	200	…	$T_2^0R_1^0$	…	…	…	…
201	202	…	$\beta^0{}_1R_1^0$	…	…	…	…
244	244.2	…	$\beta^0{}_2R_1^0$	…	…	…	…
265	265.4	…	$T_3^0\beta_1^0R_1^0$	…	…	…	…
311	311	…	R_2^0	…	…	…	…
330	330	…	$\tau(\mathrm{OH})_1^0$[c]	333	…	…	A
350.7	353	…	$T_1^0\tau(\mathrm{OH})_1^0$	…	…	…	…
354.4	354	…	$\bar{T}_2^0\tau(\mathrm{OH})_1^0$	…	…	…	…
375	377	…	$\beta_1^0\tau(\mathrm{OH})_1^0$	…	…	…	…
399	400	…	$\bar{T}_2^0\beta_1^0\tau(\mathrm{OH})_1^0$	…	…	…	…
420	422	…	$\beta_2^0\tau(\mathrm{OH})_1^0$	…	…	…	…
486	485	…	$R_1^0\tau(\mathrm{OH})_1^0$	…	…	…	…

[a]See Fig. 3 for a description of the normal modes.
[b]Reference 1.
[c]OH out-of-plane torsion based on phenol vibration assignment from Ref. 21.

perpendicular to that of the S_1 origin), marking it as the S_2 origin transition of b4HPM. There is ample vibronic level evidence to support this assignment.

Figure 10(a) shows the first 600 cm^{-1} of the DFL spectrum from the +132 cm^{-1} band of A, while Fig. 11(a) presents an overview that extends out to –1400 cm^{-1}, thereby including the activity in the ring modes. The spectrum in Fig. 11(a) is compared with the corresponding emission from the S_1 origin of b4HPM(A) [Fig. 11(b)] and with a stick spectrum of the main bands in the DFL spectrum of the S_1 origin of *p*-cresol [Fig. 11(c)] from Ebata *et al.*[19]

The spectrum in Fig. 11(a) is unusual in at least three respects. First, the spectrum is dominated by strong transitions involving ring modes at –485, –850, and –1258 cm^{-1} that are larger than the resonance fluorescence peak. These appear at positions close to the Franck–Condon active transitions in *p*-cresol[18] [Fig. 11(c)], but with an *enhanced* intensity nearly ten times the size of the corresponding bands from the S_1 origin [Fig. 11(b)]. Furthermore, there are no corresponding bands at twice these frequencies, indicating that they are not first members of long Franck–Condon progressions. This same behavior was noted in the DFL spectrum of the S_2 origin of DPM.[1]

Second, these transitions and the resonance fluorescence peak all show remarkably little activity in the torsion and butterfly modes built off them. The expanded view shown in Fig. 10(a) highlights this fact, where the T_1^0 and β_1^0 fundamentals are only about 10% the size of the resonance fluorescence, much smaller than in the S_1 origin emission. Thus, the torsional activity is *suppressed* relative to that from the S_1 origin, as occurred in DPM.[1]

Finally, a set of transitions appears with first member at –127 cm^{-1}, closely analogous to the "clump" emission identified in the S_2 origin emission in DPM beginning at –83 cm^{-1}

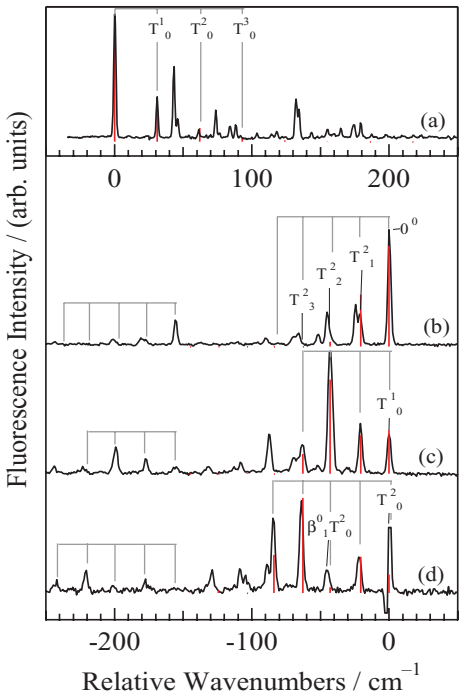

FIG. 7. (a) UV-HB spectrum, and DFL spectra from the (b) S_1 origin, and transitions (c) +31 and (d) +62 cm^{-1} above the S_1 origin, assigned to the T_0^1 and T_0^2 transitions. The stick spectra are Franck–Condon predictions using a displacement parameter D = 0.85 for the *T* mode of conformer A. The intensity of the resonance transition T_0^2 in (d) is uncertain due to the incomplete subtraction of scattered light.

in that case.[1,2] Based on the analysis in DPM, we anticipate that the bands in this region are appearing as a result of internal mixing of the S_2 origin with S_1 vibronic levels nearby in energy, that report their quantum state make-up via $\Delta v = 0$ Franck–Condon emission back to corresponding level(s) in the S_0 state.

In b4HPM, identification of the levels responsible for mixing was facilitated by the DFL spectrum shown in Fig. 10(c), due to the +117 cm^{-1} transition of b4HPM(B).

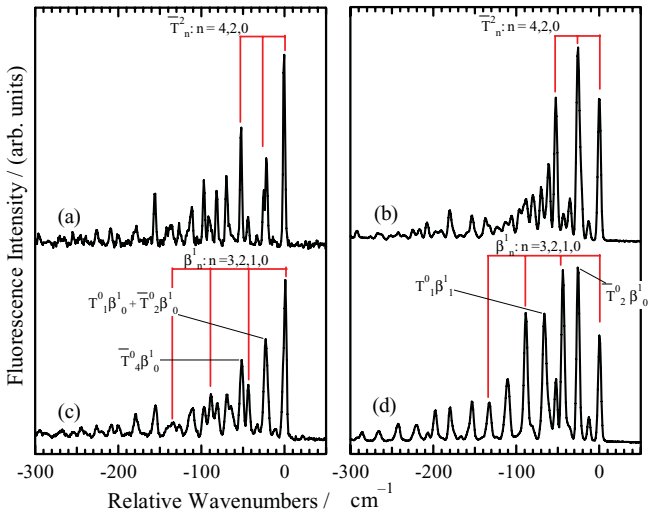

FIG. 8. DFL spectra of the (a), (b) +43 and (c), (d) +46 cm^{-1} transitions of A and B, respectively.

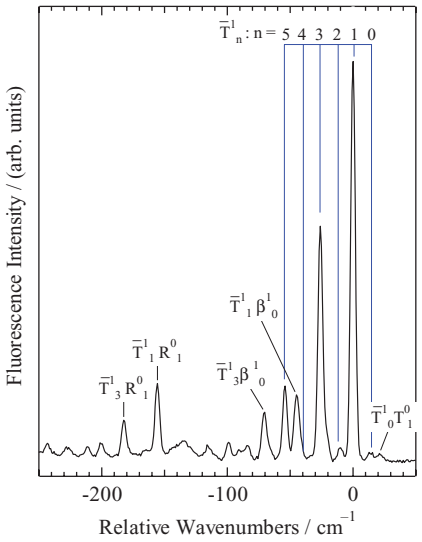

FIG. 9. DFL spectrum of the A+10.5 cm^{-1} transition assigned to the $\bar{T}_1^1$ sequence band. See text for further discussion.

This spectrum is shown rather than that from the corresponding transition in conformer A, because the transition due to B is not overlapped with b4HPM(A) transitions, and therefore provides a clearer picture of its vibronic make-up. This band, which is very weak in the excitation spectrum, has emission dominated by a false origin at –127 cm^{-1}, precisely, the frequency present in the S_2 origin emission [Fig. 10(a)]. This false origin has FC activity built off it due to torsion and butterfly modes, with intensities that are like those from the S_1 origin. Thus, a level 117 cm^{-1} above the S_1 origin in S_1 is emitting via $\Delta v = 0$ FC factors to a level 127 cm^{-1} above the S_0 zero-point level. The calculated frequencies for b4HPM (Table I) predict the frequency of the antisymmetric flapping vibration $\bar{R}$ at 127 cm^{-1}. As a result, we assign the +117 cm^{-1} band in the excitation spectrum as the S_0–S_1 $\bar{R}^1{}_0$

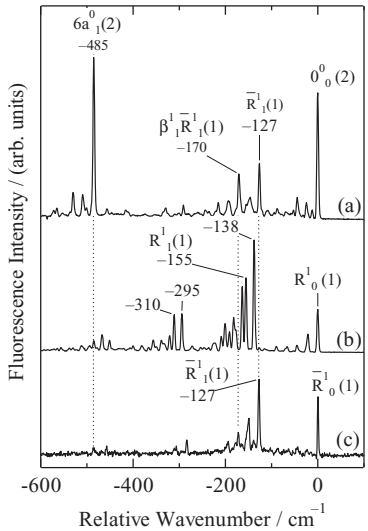

FIG. 10. DFL spectra of (a) the +132 cm^{-1} band of conformer A, (b) the +134 cm^{-1} band of conformer A, and (c) the +117 cm^{-1} band of conformer B of b4HPM. The number in parentheses indicates the excited state character (S_1 or S_2) responsible for that portion of the emission.

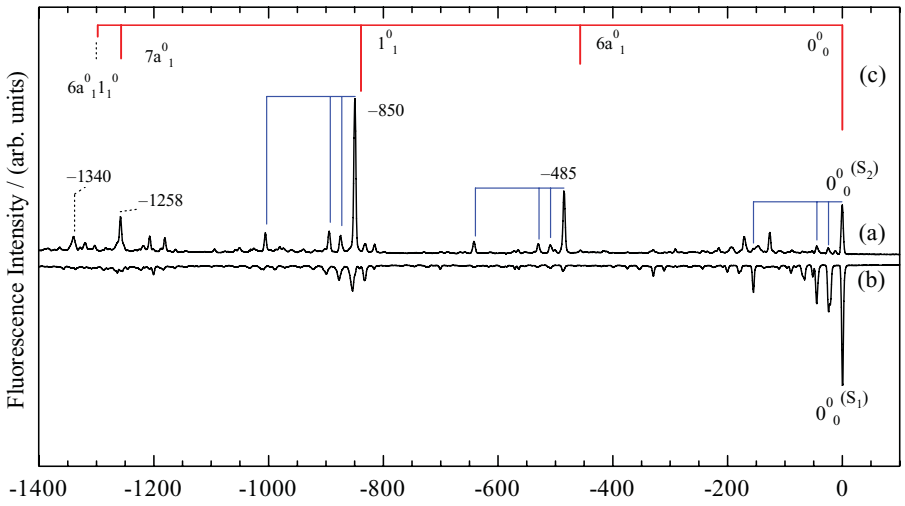

FIG. 11. (a) DFL spectrum of the (b) S_2-origin band, positioned +132 cm^{-1} above the S_1 electronic origin, of conformer A, and (c) S_1 origin, shown as an inverted trace for a better comparison. The stick spectrum shown in (a) is the DFL spectrum of the S_1 origin of *p*-cresol, generated based on experimental frequencies and intensities of Ebata *et al*. (See Ref. 18) Progressions of –24.5, –45, and –156 cm^{-1} built off of each strong transition are indicated with tie-lines (blue).

fundamental, gaining its oscillator strength by vibronic coupling to S_2 (a point to which we will return in the discussion).

The presence of the –127 cm^{-1} transition in the $S_1(v)$ emission from the (nominally) S_2 origin [Fig. 10(a)] then identifies the same $S_1\bar{R}^1$ excited state level, which is 15 cm^{-1} *below* the S_2 origin, as involved in internal mixing with the S_2 origin. Similarly, the –170 cm^{-1} transition arises from the S_1 $\bar{R}^1_1\beta^1_1$ transition to a level 170 cm^{-1} above the S_0 zero-point level (127 + 43 cm^{-1}), appearing by internal mixing of the S_2 zero-point level with S_1 $\bar{R}^1\beta^1$, also of appropriate symmetry to do so. This level is predicted to be +163 cm^{-1} from the S_1 origin (117 + 46 cm^{-1}), 31 cm^{-1} *above* the S_2 origin.

The close proximity of the +134 cm^{-1} transition in the excitation spectrum (Fig. 5) to the S_2 origin (+132 cm^{-1}) seemed to suggest that the two upper state levels might be mixed with one another. However, a high resolution scan of the +134 cm^{-1} band[6] revealed a transition dipole moment (TDM) orientation due to an S_0–$S_1(v)$ transition, and therefore, involving an upper state not of the proper symmetry to mix with the S_2 zero-point level. The inherent intensity of this transition in excitation suggests the S_0–S_1 $R^1{}_0$ transition as a possibility. Figure 10(b) presents the DFL spectrum from this band in b4HPM(A). Indeed, the emission shows a strong progression in ν_R = 155 cm^{-1}. At the same time, the dominant emission band appears at –138 cm^{-1}, reaching a ground state level 11 cm^{-1} above the 127 cm^{-1} level assigned to $\bar{R}_1$. This is precisely the frequency of the $\bar{T}$ fundamental in the ground state, leading to an assignment of the –138 cm^{-1} transition as $\bar{R}^1_1\bar{T}^1_1$. We therefore postulate that the band at –138 cm^{-1} in the dispersed fluorescence spectrum in Fig. 10(b) is present by virtue of Duschinsky mixing or Fermi resonance between the S_1 R^1 and S_1 $\bar{R}^1\bar{T}^1$ levels, where the latter level is anticipated to be close by (117 + 21.5 = 138.5 cm^{-1}) in the absence of cross anharmonicity.

The assignments just discussed identify the $S_1\bar{R}^1$ and $S_1\bar{R}^1\beta^1$ levels in S_1 as involved in internal mixing with the S_2 zero-point level, producing an excited state level of mixed character:

$$\Psi(+132\ cm^{-1}) = c_{2,000}|S_2, 0^0\rangle + c_{1,\bar{R}}|S_1, \bar{R}^1\rangle + c_{1,\bar{R}\beta}|S_1, \bar{R}^1\beta^1\rangle + \cdots.$$

As shown in greater detail in the supplementary material[5] (Fig. S2), these S_1 levels are in close proximity to the S_2 zero-point level, and dominate the $S_1(v)$ emission in Fig. 10(a). However, the overview DFL spectrum in Fig. 11(a) shows evidence of vibronic coupling much more extensive than this, producing the unusual intensity patterns observed in the ring modes and in even overtones of $\bar{T}$. Both the S_1 and S_2 emission are affected, with enhancements of ring-mode transitions from the S_2 origin occurring seemingly at the expense of a reduction in intensity in the same bands from the S_1 origin. In the Discussion section, we seek to bring all observations together into a single coherent picture via a vibronic coupling model.

V. DISCUSSION

A. Excitonic effects and internal mixing in b4HPM: Vibronic coupling model

One of the most intriguing aspects of the vibronic spectroscopy of b4HPM is the presence of, and interaction between, the two close-lying excited electronic states in this flexible bichromophore. Under jet-cooled, isolated conditions, it is possible to identify the S_0–S_1 and S_0–S_2 origins and assign a vibronic structure built off of each. Dispersed fluorescence spectra have provided state-specific insight to the vibronic coupling involving the two states, with clear spectroscopic signatures for the mixed electronic character particularly of the S_2 origin.

In this section, we compare and contrast internal mixing in b4HPM with the parent molecule DPM which we studied previously.[1] We also look in more detail at the spectroscopic manifestations of vibronic coupling between the two states.

Three intriguing aspects of the vibronic spectroscopy of b4HPM motivate our doing so. First, the excitonic splitting between S_1 and S_2 states is 132 cm^{-1} in b4HPM, a value close to that found in DPM. This occurs despite the fact that the oscillator strength of the electronic transitions in b4HPM ($f = 0.083$) is calculated to be almost 30 times greater than in DPM ($f = 0.003$). Transition dipole coupling models would therefore predict, all other things being equal, that the excitonic splitting should increase significantly in b4HPM relative to DPM. A further discussion of this issue is reserved for the rotationally resolved work to be reported elsewhere.[6]

Second, we have noted the distinct asymmetry in the intensities of Franck–Condon active modes involving the ring modes $6a$ and 1, with intensities from the S_1 origin that are much smaller than in *p*-cresol,[19] while the corresponding bands in the S_2 origin DFL spectrum are enhanced significantly, dominating the spectrum.

Finally, $\Delta v \neq 0$ transitions are far too large in transitions involving $\bar{T}$ than can be accounted for by any FC model that retains C_2 symmetry in both states (and thus has zero displacement along the nontotally symmetric $\bar{T}$ mode).

The theoretical description of vibronic coupling involving the two close-lying excited states of b4HPM shares much in common with the excitonic theory of molecular dimers. Recently, Leutwyler and co-workers have applied a linear vibronic coupling model to the 2-aminopyridine dimer,[9] thereby explaining its small excitonic splitting (11 cm^{-1} relative to a calculated splitting 40 times larger) and the complicated vibrational splittings observed in the jet-cooled excitation spectrum.

In b4HPM, the two ultraviolet chromophores are bound to one another by chemical bonds that determine the relative distance and orientation of the two chromophores. The low-frequency torsional and bending vibrations of the two phenyl rings play the same role as the intermolecular vibrations of the dimer, modulating the relative distance and orientation of the two rings, and therefore, the electronic coupling between them. As in molecular dimers, molecular bichromophores also have a subset of the higher-frequency vibrational modes that are simple sums and differences of localized vibrations of the two chromophores. Since the Franck–Condon activity of the chromophore is dictated by the geometry changes involving these modes, they serve as a basis for the description of vibronic coupling in the bichromophore.

Given this close comparison, it is worthwhile to apply a linear vibronic coupling model to b4HPM using the formalism that has been applied in past studies to molecular dimers. It is not our purpose here to recapitulate this theory, but to introduce only those elements essential for understanding the vibronic spectroscopy of flexible bichromophores, such as b4HPM and DPM,[1,2] and use it to identify and interpret the spectroscopic signatures that appear in the vibronic level excitation and dispersed fluorescence spectra.

1. Modeling the high-frequency ring modes

In b4HPM, *p*-cresol ($CH_3C_6H_4OH$) is taken as the effective monomer chromophore, and the observed Franck–Condon activity in the ring modes is used to predict the excited state displacements along symmetric monomer normal modes. Since the two chromophores in b4HPM are identical, their uncoupled energies are degenerate, and the consequent breakdown of the Born–Oppenheimer approximation requires a treatment of the vibronic energy levels and wave functions in an even-handed way that does not necessarily associate them with a single potential energy surface. Similarly, much as in a molecular dimer, a molecular bichromophore has many high-frequency normal modes that are associated with the motion of atoms localized on the two chromophores. Again, by symmetry, these normal modes are to a good approximation sums and differences of the localized vibrations of *p*-cresol.

Proceeding as before from a localized description, the wavefunctions of the bichromophore can be written as the product of electronic wavefunctions of the two rings for the ground state as $\Psi_0(q, Q_0) = \psi^A{}_0(q^A; Q^A{}_0)\psi^B{}_0(q^B; Q^B{}_0)$ and for excitation (*) on either one of the rings as $\Psi^A{}_e(q; Q_0) = \psi^{A*}(q^A; Q^A{}_0)\psi^B{}_0(q^B; Q^B{}_0)$ and $\Psi^B{}_e(q; Q_0) = \psi^A(q^A; Q^A{}_0)\psi^{B*}(q^B; Q^B{}_0)$. The linear vibronic coupling model may be expressed in terms of harmonic oscillator wavefunctions and normal coordinates, Q, as a 2×2 matrix:

$$H = \begin{bmatrix} E_{exc} + H_A + H_B + LQ_A & V_{AB} \\ V_{AB} & E_{exc} + H_A + H_B + LQ_B \end{bmatrix} \tag{1}$$

having diagonal elements that describe the vibrational Hamiltonian of one of the (localized) excited state chromophore normal modes with frequency ω_i and linear displacement LQ_i (e.g., the symmetric ring breathing mode of *p*-cresol[19]), and off-diagonal elements V_{AB} that account for the excitonic coupling between the two chromophores. The eigenvectors of Eq. (1) are the mixing coefficients, $\alpha(Q)$ and $\beta(Q)$, of the final wavefunctions, $\Psi(q; Q) = \alpha(Q)\Psi_e{}^A(q; Q) + \beta(Q)\Psi_e{}^B(q; Q)$.

In C_2 symmetry, the symmetry-adapted electronic basis functions, $\Psi^{\pm}{}_e = (1/2)^{1/2}(\Psi^A{}_e \pm \Psi^B{}_e)$, and normal coordinates, $q_{\pm} = (1/2)^{1/2}$ $(Q^A \pm Q^B)$, are most appropriate. The transcription of Eq. (1) to dimensionless elements follows that given before

$$\hbar = \begin{bmatrix} C + \frac{1}{2}(p_+^2 + q_+^2) + \frac{1}{2}(p_-^2 + q_-^2) + b_{S_+}q_+ & b_m q_- \\ b_m q_- & -C + \frac{1}{2}(p_+^2 + q_+^2) + \frac{1}{2}(p_-^2 + q_-^2) + b_{S_-}q_+ \end{bmatrix}, \tag{2}$$

where $C = V_{AB}/\hbar\omega$, and $b = (2\hbar\mu\omega^3)^{-1/2}L$. The off-diagonal elements, $b_m q_-$, mix the lower diagonal block (S^-) with the upper block (S^+) to give the S_1 and S_2 states, respectively. The subscripts on b are important only for the treatment of the inter-ring vibrational modes discussed below.

While aspects of the problem can be analyzed by considering each of the vibrations in turn within the context of the 1D model outlined in Eqs. (1) and (2), it was not possible to account for the excitonic splitting and ring-mode intensity patterns within a 1D model. As a result, a C language program was written to expand the single mode model to n vibrations.[24] Each dimension expands the column dimension (and row) by m^2, where m represents the basis set size for that vibration. Without extraordinary resources, the matrix size limits the practical use of this exact treatment to four or five vibrations with minimal basis sets. To account for each of the n vibrational frequencies, dimensionless scaling is applied as a ratio, ν_n/ν_1 to all matrix elements of that mode. In this multimode *ansatz*, it is easily verified that only one nonzero value of C is needed. Spectral predictions following diagonalization of the matrix are compared with the observed spectra after multiplication of the eigenvalues by the ν_1 fundamental frequency.

We first applied this model to address why the S_2 origin DFL intensities of the ring modes $6a$ and 1 are enhanced relative to those from the S_1 origin. Calculations using a 2D model were performed using the parameters given in Table III. The parameters include a TDM orientation that gives the 4:1 intensity ratio observed for the S_1:S_2 origins in excitation [see Fig. 5(a) and Fig. S4]. Predictions are compared with the DFL data of S_2 and S_1 in Figs. 12(a) and 12(b) and 12(c) and 12(d), respectively. Consistent with experiment, the S_2 DFL intensities of the $6a$ and 1 fundamentals are enhanced by more than five-fold relative to the resonant fluorescence intensities of the respective origins. The predictions for the excitation spectrum, shown in the supplementary material[5] (Figs. S4 and S5), are also in good agreement with the experimental UVHB spectrum of conformer A.

Inspection of the eigenvectors gives some insight into the effect of vibronic coupling. While both the S_1 and S_2 states have mixed character from each of the zero-order S^- and S^+ blocks to which they correlate, respectively, the S_2 origin is particularly affected by having more than 40% S^- character (sum of the coefficients squared) in contrast to less than 20% S^+ character in the S_1 origin. As one consequence, the ratio of the S_1:S_2 resonant fluorescence intensities increases to 6:1 from the 4:1 ratio observed in excitation. The largest impact of vibronic coupling in Fig. 12 is evident in the relative emission intensities to $6a/\bar{6}\bar{a}$ and $1/\bar{1}$. Nearly all of the S_2 origin emission character is derived from the S_1 $\bar{6}a^1$ and $\bar{1}^1$ vibronically coupled states. The corresponding negative components of emission exceed in both cases the S_2 origin intensities to $6a$ and 1 by greater than ten-fold. In contrast, the S_2 $\bar{6}a^1$ and $\bar{1}^1$ positive emission character in the S_1 state remains a minor factor in the (nominal) S_1 origin emission (by ≈ten-fold). Both the increased bias in the resonant fluorescence character and the more nearly equal weighting of S_1 character in both origins favor the enhancements observed in the ring mode-emission intensities.

TABLE III. Parameters used in the linear vibronic coupling model. The S_1:S_2 TDM components are 1.265:0.632 corresponding to a squared component ratio of 1.6:0.4 or 4:1.

Mode	b_{S-}	b_{S+}	b_m	S_0	S_1	S_2
2D			V_{AB}[a] = 154.8 cm^{-1}			
$1/\bar{1}$	0.79	0.79	0.79	850	827	827
$6a/\bar{6}\bar{a}$	0.45	0.45	0.45	485	456	456
2D			V_{AB}[a] = 45.5 cm^{-1}			
R	0.72	0.22	0.065	156	134	134
$\bar{R}$				126	120	120
T	0.85	0.5	0.04	20.7	30.8	30.8
$\bar{T}$				11.7	22.7	22.7

[a]The vertical splitting is 2 V_{AB}.

2. The inter-ring modes $R/\bar{R}$ and $T/\bar{T}$

The inter-ring modes shown in Figs. 3(b)–3(e) form two symmetric/antisymmetric pairs due to phenyl ring flapping ($R/\bar{R}$) and torsion ($T/\bar{T}$). These modes are not localized on each of the rings, but can nevertheless be thought of as simple sums and differences of localized motions that reorient the two rings with respect to one another. We therefore postulate that these two pairs of vibrations can be treated in the framework of the linear vibronic coupling model in much the same way as the ring modes ($6a$ and 1) themselves, and test this postulate against the observed intensity patterns involving these modes in the excitation and dispersed fluorescence.

The results of initial 2D calculations using b parameters determined from the experimental Franck–Condon activity in R and T fails at all levels to account for the observed UVHB spectrum (see Fig. S5). The close proximity of the $R/\bar{R}$ mode pair to the S_2 origin causes severe vibronic coupling to occur and results in splitting of the $\bar{R}^1_0$ and S_2 0^0_0 bands by ≈60 cm^{-1} to either side of the observed positions. To account for observations, a phenomenological approach is taken to dampen the coupling by introducing an independent b value (b_m) for the off-diagonal blocks shown in Eq. (2). Reducing the value of b_m for the $R/\bar{R}$ mode pair relative to the on-diagonal b values effectively reduces the coupling between the S^- and S^+ blocks. The independent on-diagonal values (b_{S-}, b_{S+}) are then free to reproduce the observed FC activity in the S_1 and S_2 states. The modified model predictions are shown in comparison with the UVHB spectrum and origin DFL spectra of conformer A in Fig. 13. Determinations of b_{S-} and b_{S+} were first estimated from the S_1 and S_2 DFL data. Then b_m and C were iteratively varied until the intensities and positions of the $R/\bar{R}$ and S_2 origin bands came into close agreement with experiment. The parameters are summarized in Table III. The b_m value for $R/\bar{R}$ is 0.065, nearly an order of magnitude smaller than the on-diagonal elements. This analysis clearly shows that this inter-ring mode pair is much less efficient in its vibronic coupling than the ring modes themselves.

Thus, even though emission involving the $\bar{R}$ mode played a key role in identifying the presence of vibronic coupling in

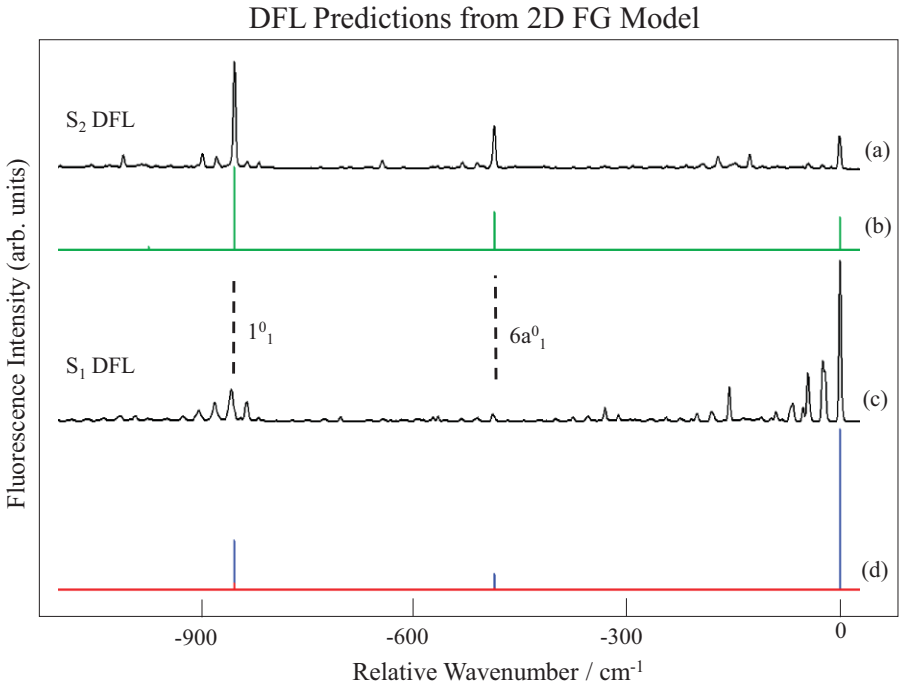

FIG. 12. Comparison of the experimental DFL spectra from the (a) S_2 and (c) S_1 origins with the best-fit results (b, (d) from the 2D vibronic coupling model for the ring modes $6a/\bar{6}\bar{a}$ and $1/\bar{1}$. See text for further discussion.

the S_2 origin emission [Fig. 10(a)], vibronic coupling induced by reorientation of the aromatic rings along the R and $\bar{R}$ vibrations is not as efficient as that predicted by the model for the ring modes $6a$ and 1. In this sense, vibronic coupling involving $\bar{R}$ gains prominence primarily due to the close proximity of the S_1 $\bar{R}^1$ level to the S_2 origin, and not by virtue of any inherent strength of its vibronic coupling matrix element.

In contrast, the reduction of the off-diagonal b_m value for the $T/\bar{T}$ mode pair has less impact on the intensities and positions of transitions involving T and $\bar{T}$, presumably due to the larger energy gap between the frequencies of the $T/\bar{T}$ pair (31/21 cm^{-1}) and S_1–S_2 splitting (132 cm^{-1}). Vibronic coupling involving the phenyl torsional modes should appear in much the same way as for the $R/\bar{R}$ pair, enhancing

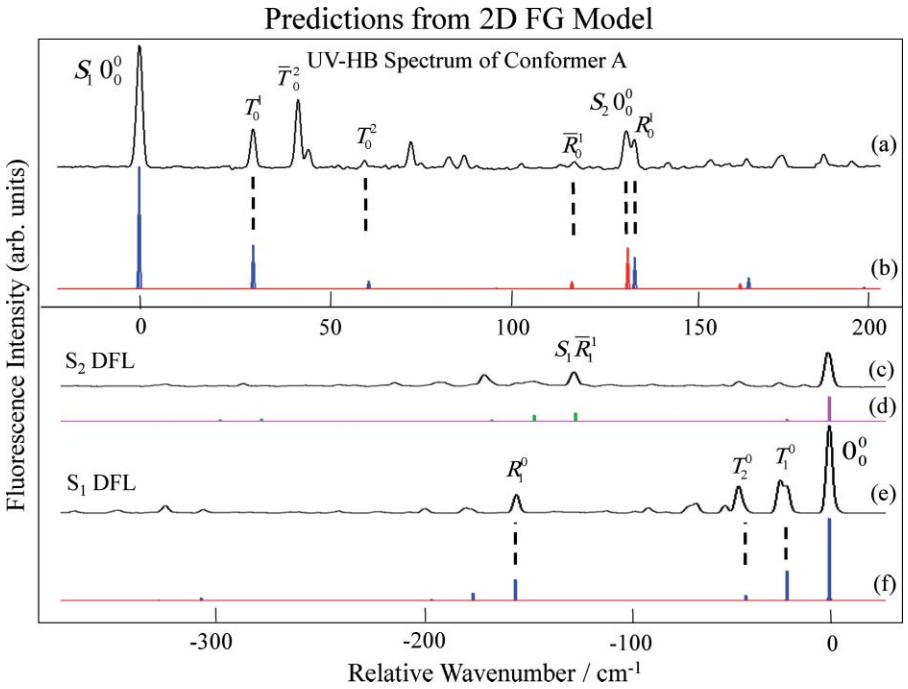

FIG. 13. Comparison of the experimental (a) UV-HB, (c) S_1 DFL, and (e) S_2 DFL origin spectra with the corresponding best-fit results (b), (d), (f) from the 2D vibronic coupling model for the inter-ring modes $R/\bar{R}$ and $T/\bar{T}$. The mode labeled $S_1\bar{R}_1^1$ in the S_2 DFL spectrum is the position of the $\bar{R}_1^0$ mode that gains its oscillator strength from vibronic coupling with S_1. See text for further discussion.

intensity in emission to the $\bar{T}$ fundamental at –11 cm^{-1}. However, this emission is not observed. Instead, the experimentally observed anomaly involved the $\Delta v = \pm 2$ transitions in $\bar{T}$, which are far too intense to be accounted for by the Franck–Condon activity.

Thus, inclusion of the inter-ring modes in the model as vibrational pairs on the same footing as the ring modes appears not to be fully justified, suggesting that further refinement of the model is needed for their proper description. One possible extension would involve inclusion of a quadratic term in the vibronic coupling involving the $T/\bar{T}$ pair, leading to a turn-on in $\Delta v = \pm 2$ transitions. The simplifying assumption that the uncoupled vibrations in each pair have the same frequency in S_0, S_1, and S_2 states also needs to be evaluated, since the $R/\bar{R}$ and $T/\bar{T}$ pairs have frequencies that change significantly upon electronic excitation (I). Furthermore, the ring modes are only mildly perturbed by the presence of the second ring, while the inter-ring mode frequencies are defined by their interaction. Such refinements are left for future work.

VI. CONCLUSIONS

The present study of the vibronic spectroscopy of b4HPM has led to a detailed characterization of the levels involved in vibronic coupling between the close-lying S_1 and S_2 states of this flexible bichromophore. The emission from the S_0–S_1 and S_0–S_2 origins, which are separated by only 132 cm^{-1} from one another, shows a detailed evidence of the states most directly involved in the mixing. In summarizing the important conclusions to be drawn from this work, it is also useful to compare vibronic coupling in b4HPM and DPM.

Table IV summarizes and compares key aspects of the vibronic coupling in b4HPM and DPM. It is clear from the comparison that many aspects of the vibronic coupling are retained between the two molecules. Both the splitting between S_1 and S_2 origins (123 cm^{-1} in DPM vs 132 cm^{-1} in b4HPM) and the S_1:S_2 intensity ratio (5:1 vs 4:1) are nearly the same in the two molecules. The much greater inherent oscillator strength of the cresol chromophore over that of toluene would suggest a much larger splitting for b4HPM than DPM. However, the similar splitting can be accounted for by a detailed consideration of the changes in the localized TDM orientations determined from rotationally resolved UV analyses of the S_1 origins.[6] A simple transition dipole interaction model based on these results gives a splitting that is four-fold smaller than that in DPM. Further reduction of the excitonic interactions may derive from the damping factors needed to model the inter-ring modes in b4HPM.

TABLE IV. Comparison of vibronic coupling in b4HPM and DPM.

Property	DPM	b4HPM
Observed S_1-S_2 splitting	123 cm^{-1}	132 cm^{-1}
Calculated vertical splitting	391 cm^{-1}	(420–462)[a] cm^{-1}
I(S_2 origin): I(S_1 origin)	≈5:1	≈4:1
Emission from S_2 origin to $\bar{6}a_1^0$ and $\bar{1}_1^0$	Strongly enhanced	Strongly enhanced
Mixing of S_2 origin with S_1(v) levels nearby	Due to ($T\ \bar{T}\ \beta$) levels of right symmetry within $\Delta E = \pm 10$ cm^{-1}	Due to $\bar{R}^1$ and $\bar{R}^1\beta^1$ levels split –10 and +28 cm^{-1} from the S_2 0_0^0.
Intensity of $\Delta v(\bar{T}) = \pm 2$ transitions	Weaker, skewed to $\bar{T}^n_{n+2}$ in emission	Strong, symmetrical

[a]Range of values for uu, dd, and ud(du) conformers.

The strongly enhanced intensity of emission from the S_2 origin to the $\bar{6}a_1^0$ and $\bar{1}_1^0$ fundamentals is also present in both molecules. In our earlier study of DPM, we noted this fact, but lacked an explanation for it. Here the multimode linear vibronic coupling model developed in this work is used to prove that this enhancement in the S_2 origin emission to the $\bar{6}a$ and $\bar{1}$ fundamentals is accompanied by a corresponding reduction in intensity in the $6a^0_1$ and 1^0_1 transitions from the S_1 origin, and both effects are a characteristic signature of vibronic mixing involving these modes. Comparison of the spectra of b4HPM with *p*-cresol identified these same transitions as the ones carrying strong Franck–Condon activity in the single chromophore, and proves that the linear vibronic coupling model can be used to account for this emission. The final result of this modeling is that the S_2 origin is in fact a highly mixed S_2/S_1 level with substantial components from S_1 $\bar{6}a^1$ and $\bar{1}^1$.

In addition to this mixing involving the Franck–Condon active ring modes, there is weaker mixing involving low-frequency inter-ring modes that are in close proximity to the S_2 origin. In DPM, this additional mixing involved ($T\ \bar{T}\ \beta$) levels with quantum make-up (050), (230), (410), and (011). These levels are a set nearest in energy to the S_2 origin of the correct symmetry to couple to it (odd quanta in $\bar{T}$). Since many of these levels involve $\Delta v(\bar{T}) > 1$, this mixing cannot be accounted for by a linear vibronic coupling model, and was previously ascribed to higher-order terms in the Herzberg–Teller vibronic coupling scheme.[25] In b4HPM, OH substitution in the *para* positions on the ring has dropped the frequency of the ring flapping vibration $\bar{R}$ (117 cm^{-1} in S_1) so that its fundamental falls in close proximity to the S_2 origin (+132 cm^{-1}). This level now dominates the near-resonant S_2/S_1 mixing, producing emission ascribable to S_1 $\bar{R}^1_1$, with upper state located 15 cm^{-1} below the S_2 origin. Analogous emission from S_1 $\bar{R}^1_1\beta^1_1$ is also prominent in the emission, arising from an upper state located 29 cm^{-1} above the S_2 origin. Interestingly, this near-resonant mixing between S_2 0^0 and S_1 $\bar{R}^1$ is predicted by the linear vibronic coupling model to be much larger than that observed given the Franck–Condon activity in its symmetric partner S_1 R^1_0. A phenomenological damping is able to bring observation and model into agreement. We postulate that the ring-flapping modes R and $\bar{R}$ do not modulate the electronic coupling between the two rings significantly. However, a full physical understanding of the damping in coupling awaits further theoretical work.

Finally, the phenyl torsional modes also appear to be involved in vibronic coupling in a way that cannot be accounted for by a linear vibronic coupling model. The most prominent observed effect is the greatly increased intensity in the $\Delta v = \pm 2$ transitions involving $\bar{T}$ despite the almost complete lack of a $\Delta v = \pm 1$ counterpart anticipated by the

model. The enhanced $\Delta v = \pm 2$ emission was also observed in DPM, but to a lesser degree. Inclusion of quadratic coupling terms in the vibronic coupling model [Eqs. (1)–(2)] may be necessary to account for observation. The antisymmetric phenyl torsion $\bar{T}$ maintains a nearly 90° relative orientation between the two phenyl rings, and thus might not be anticipated to be a strong mechanism for vibronic coupling. These phenyl torsional modes are probed in greater detail in our studies of conformational isomerization in b4HPM.

ACKNOWLEDGMENTS

C.P.R., N.R.P., and T.S.Z. gratefully acknowledge the support from the Department of Energy Basic Energy Sciences, Division of Chemical Sciences under Grant No. DE-FG02–96ER14656. C.W.M. would like to thank the "Deutsche Akademie der Naturforscher Leopoldina" for a postdoctoral scholarship (Grant No. BMBF-LPD 9901/8–159 of the "Bundesministerium für Bildung und Forschung"). C.P.R. and T.S.Z. thank Evan Buchanan for the support given with some UVD and RIDIR experiments, and Dr. Lyudmila Slipchenko for help with Q-CHEM calculations.

[1] N. R. Pillsbury, J. A. Stearns, C. W. Müller, D. F. Plusquellic, and T. S. Zwier, J. Chem. Phys. **129**, 114301 (2008).
[2] J. A. Stearns, N. R. Pillsbury, K. O. Douglass, C. W. Müller, T. S. Zwier, and D. F. Plusquellic J. Chem. Phys. **129**, 224305 (2008).
[3] N. R. Pillsbury, C. W. Müller, W. L. Meerts, D. F. Plusquellic, and T. S. Zwier, J. Phys. Chem. A **113**(7), 5000 (2009).
[4] A. Amirav, U. Even, and J. Jortner, Chem. Phys. Lett. **69**, 14 (1980); J. Chem. Phys. **74**, 3745 (1981); S. M. Beck, D. E. Powers, J. B. Hopkins, and R. E. Smalley, *ibid.* **73**, 2019 (1980); J. O. Berg, Chem. Phys. Lett. **41**, 547 (1976); J. Jortner, Faraday Discuss. **108**, 1 (1997); P. Wannier, P. M. Rentzepis, and J. Jortner, Chem. Phys. Lett. **10**, 193 (1971).
[5] See supplementary material at http://dx.doi.org/10.1063/1.3580901 for conformation-specific fluorescence dip infrared (FDIR) spectroscopy results, Fermi resonance mixing in conformer B, S_1 vibronic levels near the S_2 electronic origin, and intensity predictions for the excitation spectrum of conformer A.
[6] S. G. Chou, C. P. Rodrigo, C. W. Müller, K. O. Douglass, T. S. Zwier, and D. F. Plusquellic, J. Phys. Chem. A (2011) (in press).
[7] C. P. Rodrigo, C. W. Müller, D. F. Plusquellic, and T. S. Zwier (unpublished).
[8] M. Andrzejak and P. Petelenz, Chem. Phys. **335**(2–3), 155 (2007); R. L. Fulton and M. Gouterman, J. Chem. Phys. **35**(3), 1059 (1961); **41**, 2280 (1964).
[9] P. Ottiger, S. Leutwyler, and H. Köppel, J. Chem. Phys. **131**, 204308 (2009).
[10] T. S. Zwier, J. Phys. Chem. A **105**, 8827 (2001).
[11] Certain equipment or materials are identified in this paper in order to specify the experimental procedure adequately. Such identification is not intended to imply endorsement by the National Institute of Standards and Technology, nor is it intended to imply that the materials or equipment identified are necessarily the best available..
[12] P. K. Weiner and P. A. Kollman, J. Comput. Chem. **2**, 287 (1981).
[13] F. Mohamadi, N. G. J. Richards, W. C. Guida, R. Liskamp, M. Lipton, C. Caufield, G. Chang, T. Hendrickson, and W. C. Still, J. Comput. Chem. **11**, 440 (1990).
[14] A. D. Becke, J. Chem. Phys. **98**, 5648 (1993); C. T. Lee, W. T. Yang, and R. G. Parr, Phys. Rev. B **37**, 785 (1988).
[15] Y. Zhao and D. G. Truhlar, J. Chem. Theory Comput. **2**, 1009 (2006); **3**, 289 (2007); Acc. Chem. Res. **41**, 157 (2008).
[16] J.-D. Chai and M. Head-Gordon, Phys. Chem. Chem. Phys. **10**, 6615 (2008).
[17] M. J. Frisch, G. W. Trucks, H. B. Schlegel *et al.*, GAUSSIAN 03, Revision E.01, Gaussian, Inc., Wallingford, CT, 2004; GAUSSIAN 09, Gaussian, Inc., Wallingford, CT, 2009.
[18] Y. Shao, L. Fusti-Molnar, Y. Jung *et al.*, Q-CHEM, Q-Chem, Inc., Pittsburgh, PA, 2007.
[19] T. Ebata and M. Ito, J. Phys. Chem. **96**, 3224 (1992).
[20] G. A. King, A. L. Devine, M. G. D. Nix, D. E. Kelly, and M. N. R. Ashfold, Phys. Chem. Chem. Phys. **10**, 6417 (2008).
[21] G. Varsanyi, *Assignments for Vibrational Spectra of 700 Benzene derivatives* (Wiley, New York, 1974).
[22] W. Roth, P. Imhof, M. Gerhards, S. Schumm, and K. Kleinermanns, Chem. Phys. **252**(1–2), 247 (2000).
[23] J. R. Henderson, M. Muramoto, and R. Willett, J. Chem. Phys. **41**, 580 (1964).
[24] The source code is available upon request from the authors.
[25] M. Bixon and J. Jortner, J. Chem. Phys. **48**, 715 (1968); J. Jortner and R. S. Berry, J. Chem. Phys. **48**, 2757 (1968); A. Nitzan and J. Jortner, J. Chem. Phys. **56**, 3360 (1972); B. Sharf, Chem. Phys. Lett. **8**, 391 (1971); B. Sharf and R. Silbey, Chem. Phys. Lett. **9**, 125 (1971).